Soil Biology and Biochemistry 172 (2022) 108743

Contents lists available at ScienceDirect

Soil Biology and Biochemistry

journal homepage: www.elsevier.com/locate/soilbio

Climate-induced shifts in composition and protection regulate temperature sensitivity of carbon decomposition through soil profile

Xiali Mao [a,1], Jinyang Zheng [a,1], Wu Yu [a,b], Xiaowei Guo [a], Kang Xu [a], Ruiying Zhao [a], Liujun Xiao [a], Mingming Wang [a], Yefeng Jiang [a], Shuai Zhang [a], Lun Luo [c], Jinfeng Chang [a,d,e], Zhou Shi [a,d,e], Zhongkui Luo [a,d,e,*]

[a] Institute of Agriculture Remote Sensing and Information Technology, College of Environmental and Resource Sciences, Zhejiang University, Hangzhou, 310058, China
[b] College of Resources and Environment, Tibet Agricultural and Animal Husbandry University, Nyingchi, Tibet, 860100, China
[c] South-East Tibetan Plateau Station for Integrated Observation and Research of Alpine Environment, Institute of Tibetan Plateau Research, Chinese Academy of Sciences, Nyingchi, Tibet, 860100, China
[d] Academy of Ecological Civilization, Zhejiang University, Hangzhou, 310058, China
[e] Key Laboratory of Environment Remediation and Ecological Health of Ministry of Education, Zhejiang University, Hangzhou, 310058, China

ARTICLE INFO

Keywords:
Carbon models
Climate change
Carbon compounds
Deep soil
Warming
Q_{10}

ABSTRACT

Through soil profile, both chemical composition of soil organic carbon (SOC) and edaphic physiochemical properties present a vertical gradient, likely resulting in depth-specific SOC dynamics in response to climate change (e.g., global warming). We assessed temperature sensitivity of SOC decomposition (Q_{10}) by incubating (128 days) soils sampled across five sequential layer depths (i.e., 0–10, 10–20, 20–30, 30–50, and 50–100 cm) at ten sites along a ~2500 m elevational transect (from ~2100 m to ~4600 m) covering various vegetation types (from evergreen broadleaved forest to alpine meadow) in southeast Tibet, China. The Q_{10} of SOC decomposition was significantly affected by both soil depth and elevation. However, depth-induced variation of Q_{10} was much smaller than that induced by the elevation gradient. Across the ten sites and five soil depths, chemical composition of SOC and its physiochemical protection against decomposition contributed >80% to the explained variance of Q_{10} values. Path analysis suggested that climate indirectly affected Q_{10} via its regulation on chemical composition of SOC and their physiochemical stabilization. The results from a carbon model constrained by the collected data further revealed that fast, slow and passive SOC pools exhibited significant difference in their Q_{10}, resulted from different involvement of chemical composition and physicochemical protection in their decomposition. Our findings demonstrate similar temperature sensitivity of SOC decomposition across soil depths, but spatially heterogeneous temperature sensitivity due to climate-induced variability of both chemical recalcitrance of SOC and its physiochemical protection against decomposition.

1. Introduction

The fate of soil organic carbon (SOC) under climate warming is a vital determinant of carbon cycle-climate feedbacks. Kinetic theory suggests that temperature sensitivity of the decomposition of an organic-carbon substrate is a function of its molecular structure (i.e., intrinsic temperature sensitivity) (Davidson and Janssens, 2006). More complex molecules usually have higher activation energy and, hence, higher intrinsic temperature sensitivity. However, physical or chemical protection (e.g., binding with soil minerals and occlusion in soil aggregates), together with various environmental constraints, can dampen or obscure the intrinsic temperature sensitivity by reducing substrate availability (Dungait et al., 2012). This complexity would be a key reason for large prediction uncertainties in SOC dynamics by Earth system models which usually predict the temperature sensitivity of SOC decomposition based on relatively simple temperature response functions (e.g., Q_{10} or Arrhenius functions) due to our poor understanding of underlying mechanisms (Jackson et al., 2017; Xu et al., 2021). We need

* Corresponding author. Institute of Agriculture Remote Sensing and Information Technology, College of Environmental and Resource Sciences, Zhejiang University, Hangzhou, 310058, China.
E-mail address: luozk@zju.edu.cn (Z. Luo).
[1] Equal contribution.

https://doi.org/10.1016/j.soilbio.2022.108743
Received 18 December 2021; Received in revised form 24 May 2022; Accepted 29 May 2022
Available online 2 June 2022

to elucidate and disentangle the specific role of molecular structure, physiochemical protection and their interactions with environmental conditions in regulating the temperature sensitivity of SOC decomposition.

A number of studies have been conducted to assess the temperature sensitivity of SOC decomposition and underlying mechanisms in different ecosystems (Jackson et al., 2017; Xu et al., 2021). However, temperature sensitivity of SOC decomposition greatly vary not only across space and over time but also through soil depths. The majority of SOC stores in subsoil below 0.3 m (Jobbagy and Jackson, 2000; Li et al., 2020), which has been found to show similar temperature sensitivity as topsoil SOC (Hicks Pries et al., 2017). Hence, depth-resolved assessment is growing due to rising concern of subsoil SOC loss under warming (Li et al., 2018, 2020; Qin et al., 2019; Vaughn and Torn, 2019). A short-term incubation experiment (21 h) using soil samples down to 1 m from 90 upland forests in China suggested that SOC in deeper layers is more sensitive to temperature (Li et al., 2020). They further found that climate is consistently the dominant regulator of the variability of the temperature sensitivity across the sites in all soil depths, while chemical recalcitrance (which is indicated by the ratio of carbohydrates to aromatics) also plays an important regulating role in deeper layers. On the contrary, a long-term incubation (330 days) of permafrost soils from Tibet, China, found weaker temperature sensitivity of SOC in deeper layers due to stronger aggregate protection and lower microbial activity (Qin et al., 2019). Using radiocarbon signals to divide mineralized carbon (i.e., CO_2) into that derived from young (decades in terms of carbon age) and old SOC (millennia), Vaughn and Torn (2019) revealed that SOC in different depths with distinct ages responds similarly to warming (i.e., equal temperature sensitivity to warming) and suggested that chemical recalcitrance of SOC might be secondary for the temperature sensitivity of SOC mineralization. Overall, controlling factors underpinning the variable temperature sensitivities of SOC decomposition across soil depths need to be further elucidated to improve our understanding of temperature sensitivity of whole-profile SOC decomposition.

Soil organic carbon is comprised of numerous compounds that have distinct turnover behaviors and persistence. A potential solution to reduce uncertainties in our understanding of how SOC responds to temperature would be to align temperature responses with diverse and functionally distinct carbon compounds. Particulate (POC) and mineral-associated organic carbon (MOC) are two such functionally contrasting pools reflecting both molecular structure and physiochemical protection (Lavallee et al., 2020). Large-scale studies have demonstrated that the two pools show distinct accumulation and turnover behaviors (Cotrufo et al., 2019; Luo et al., 2020). However, POC and MOC are primarily distinguished by particle size. Given the complexity of SOC composition, direct information of molecular characteristics may add another layer of information for understanding SOC temperature sensitivity. Indeed, a continental scale assessment of molecular composition of SOC revealed that environmentally and geochemically associated trade-offs in soil carbon molecular composition could well explain the spatial variability of SOC storage (Hall et al., 2020). Integrating information of various SOC pools with processes involved in physiochemical protection of SOC may shed new lights on mechanistic understanding of the temperature sensitivity of SOC decomposition (Davidson and Janssens, 2006). This is particularly relevant to depth-resolved prediction of SOC dynamics as both physiochemical protection and molecular structure of organic carbon substrates may present a gradient through soil profile (Qin et al., 2019).

The Tibet Plateau, also called the world's "third pole", stores a large amount of SOC (27.75 Pg in the top 1 m soil) (Wang et al., 2021) which has been predicted to be very sensitive and vulnerable to climate warming (Guan et al., 2018; Pei et al., 2022). In addition, the mountainous environment of this region leads to heterogenous edaphic properties, distinct climatic conditions, and diverse vegetation covers (Xu et al., 2021), providing a good opportunity to explore the spatial variability of depth-resolved temperature sensitivity of SOC decomposition. In this study, we collected soil samples from five sequential soil layer depths (i.e., 0–10, 10–20, 20–30, 30–50 and 50–100 cm) at ten sites across an elevational gradient ranging from ~2100 m to ~4600 m in southeast Tibet. These sites cover diverse of climate, vegetation types (from evergreen broadleaved forest to alpine meadow) and soil conditions. Together with measurements of a suite of chemical and physical pools of SOC, laboratory soil incubation (128 days) and pool-based modelling, we aim to evaluate the temperature sensitivity of total SOC decomposition as well as different carbon pools distinguished by turnover rates, and distinguish the specific regulating role of chemical composition and physiochemical protection in the variability of Q_{10} across elevations and soil depths.

2. Materials and methods

2.1. Study sites and soil sampling

We selected an elevational transect in southeastern Tibet to sample soils. The elevation of the transect ranges from ~2100 m to ~4600 with a mean annual temperature (MAT) ranging from −0.27 to 11.04 °C and mean annual precipitation (MAP) ranging from 624 to 888 mm. This transect locates in a remote area in Tibet and keeps natural landscape with few human activities. The soils collected from elevations of 4600 m–4300 m, 4300 m–4000 m, 4000 m–3400 m, and 3400 m–2100 m belong to Matti-Gelic Cambisol, Albic Umbri-Gelic Cambisol, Dystric Podzoluvisol and Eutric Cambisol, respectively (Li et al., 2014; Xu et al., 2021). A brief introduction of the study sites and basic soil properties have been presented in Table 1.

In September 2020, we took soil cores down to 1 m with five depth intervals (i.e., 0–10, 10–20, 20–30, 30–50, and 50–100 cm) from ten sites along the transect (Table 1) using a combined gradient and replicated sampling design (Kreyling et al., 2018). Among the ten sites, we set up three 10 × 10 m sampling quadrats (as three replicates) approximately 100 m apart at the elevations of 2100, 2762, 3448, 4090 and 4559 m. At other elevations (i.e., 2326, 3078, 3611, 4308 and 4369 m), we only set up one 10 × 10 m sampling quadrat. At each quadrat, five randomized soil profiles were collected and subsequently mixed to get one composite sample by depth. This design allows us to cover more gradients, particularly considering the laborious challenge at high altitudes. Soil samples were stored in airtight polypropylene bags and placed in a cooler filled with ice-cubes during transportation to the laboratory. After transporting to laboratory, the soil samples were sieved to 2 mm to remove stones and visible roots. Then, the composite sample was divided into two subsamples in laboratory: one air-dried for determining soil physicochemical properties, and the other temporarily stored at 4 °C for later laboratory respiration incubation and measurements of microbial biomass carbon and dissolved organic carbon within two weeks. Using the samples, we measured a series of variables relating to edaphic properties, chemical composition and physical protection of SOC (Table 2).

2.2. Soil temperature

Soil temperature at each soil depth at the ten sampling sites were automatically monitored and recorded every 4 h for one year, by placing data loggers (iButton; model DS 1921G, Dallas Semiconductor, TX, USA) to the middle of each of the five soil layer depths at the time of soil sampling (September 2020). iButtons were retrieved in October 2021 to download temperature records which were used to calculate annual mean soil temperature (SoilT), mean temperature in the warmest month (August, SoilTw), and mean temperature in the coldest month (February, SoilTc; Table 2).

2.3. Edaphic properties and SOC compounds

We determined the following edaphic variables using standard

Table 1
Soil sampling sites and soil properties in the top 10 cm soil.

Vegetation	Elevation (m, a. s.l.)	Coordinates	MAT (°C)	MAP (mm)	Dominant species	SOC (g kg^{-1} soil)	TN (g kg^{-1} soil)	pH	Silt + Clay (%)
Alpine meadow	4559	94°39′8″E 29°36′41″N	−0.28	624	*Polygonum macrophyllum* *Potentilla peduncularis*	69.67 ± 10.37	5.34 ± 0.61	5.01 ± 0.02	50.39 ± 4.51
Alpine bush	4369	94°43′5″E 29°34′6″N	0.62	631	*Rhododendron bulu* *Potentilla fruticosa*	57.70	4.27	4.92	53.70
Alpine shrub	4308	94°43′36″E 29°35′14″N	1.63	637	*Rhododendron aganniphum*	88.60	3.62	4.64	52.54
Evergreen coniferous forest	4090	94°43′30″E 29°35′37″N	2.67	645	*Abies georgei* *Rosa omeiensis*	65.00 ± 1.03	3.66 ± 0.16	4.75 ± 0.17	56.10 ± 1.46
	3611	94°43′52″E 29°36′34″N	4.41	661	*Abies georgei* *Sorbus rehderiana*	64.90	3.70	4.72	52.06
Evergreen broadleaved-coniferous mixed forest	3448	94°44′15″E 29°46′20″N	5.83	666	*Picea likiangensis* *Quercus aquifolioides*	79.17 ± 19.82	4.60 ± 0.98	4.90 ± 0.14	64.47 ± 5.77
	3078	95°43′27″E 29°50′38″N	6.30	777	*Picea likiangensis* *Betula utilis*	60.10	3.88	5.47	55.30
Evergreen coniferous forest	2762	95°43′58″E 29°52′27″N	8.03	845	*Pinus armandii* *Rosa sericea*	56.60 ± 0.15	2.51 ± 0.18	5.54 ± 0.23	53.59 ± 4.07
Evergreen broadleaved-coniferous mixed forest	2326	95°5′53″E 30°6′16″N	10.89	868	*Pinus armandii* *Alnus nepalensis*	54.80	3.77	5.77	51.24
Evergreen coniferous forest	2070	95°1′40″E 30°7′43″N	11.04	888	*Alnus nepalensis*	17.03 ± 2.83	1.01 ± 0.05	8.49 ± 0.18	25.62 ± 0.17

Note: A gradient sampling design was adopted to cover more elevations (Kreyling et al., 2018). Values for soil properties at elevations of 4559, 4090, 3448, 2762, 2070 m are given as mean ± standard error (n = 3), at other elevations only is the value for one composite sample given.

methods: SOC, total nitrogen (TN), inorganic N (NO_3^--N and NH_4^+-N), total phosphorus (TP), available phosphorus (AP), soil pH, texture, Fe and Al oxides, moisture content and soil bulk density (BD). Using the air-dried samples, SOC and soil TN were analyzed with an elemental analyzer (Elementar Vario EL Cube, Germany) after treating with HCl to remove carbonate. Soil NH_4^+-N, NO_3^--N and AP were analyzed by an UV spectrophotometer (Shimadzu, UV-2450, Japan). Soil pH was measured using deionized water in a 1:2.5 (w: v) soil-water suspension with a pH electrode (Mettler-Toledo, Switzerland). Soil texture was determined using a laser particle size analyzer (LS-CWM, OMEC, China) after full dispersion of the sample with HCl and then H_2O_2 to remove carbonate and organic matter. The free oxides (i.e., Fed, Ald) and amorphous oxides (Feo, Alo) were extracted with dithionite-citrate-bicarbonate solution and ammonium-oxalate solution, respectively, and then digested with H_2SO_4 and H_2O_2. Fe and Al concentrations in digested solutions were analyzed by inductively coupled plasma optical emission spectroscopy (Optima, 2000, PerkinElmer Co., USA). Soil moisture was determined by drying fresh soil samples in an oven at 105 °C until constant weight obtained and dry weight of the sample recorded. The core ring sampler (5 cm diameter, 100 cm^3 volume) was dried at 105 °C for 48 h, then weighed and corrected for gravels (>2 mm) for BD determination. The SOC stock (SOCs) was then calculated as:

$$SOCs = SOC \times BD \times D \times \left(1 - \frac{Gr}{100}\right), \quad (1)$$

where SOC, BD, Gr and D denote the SOC concentration (g kg^{-1}), bulk density (g cm^3) of the fine earth fraction < 2 mm, volume percentage of gravel (%) and thickness (cm) of each soil horizon.

Dissolved organic carbon (DOC) was extracted with deionized water at a ratio of 1:2.5, shaken for 30 min and then filtered through a 0.45 μm membrane. Soil microbial biomass carbon (MBC) was determined after the chloroform fumigation-extraction. Specifically, 5 g fresh soil was fumigated with chloroform for 24 h and another 5 g soil kept non-fumigated. Both the fumigated and non-fumigated soil samples were extracted with 20 mL 0.5 M K_2SO_4, shaken for 30 min and then filtered through a 0.45 μm membrane. MBC content was calculated as the difference between organic carbon in fumigated and unfumigated samples, corrected using a conversion factor of 0.45 for unrecovered biomass (Vance et al., 1987). By drawing standard curves, the filtrates above were all analyzed for organic carbon using a TOC analyzer (Multi N/C 3100, Germany).

To determine the relative contribution of MOC versus POC fraction to total SOC, all soil samples were fractionated by size (0.053 mm) after full soil dispersion (Six et al., 1998). Briefly, air-dried soils were sieved to 2 mm, and 5 g soil was shaken in dilute (0.5%) sodium hexametaphosphate and beads for 18 h to completely disperse the soil. The dispersed soil was then rinsed onto a 0.053 mm sieve and the fraction passing through (<0.053 mm) was collected as MOC; the fraction remaining on the sieve was collected as POC. After drying to constant weight in a 60 °C oven, each fraction was analyzed for carbon concentration in an elemental analyzer (Elementar Vario EL Cube, Germany). Standard reference soil (Certified reference material, GBW07448) was measured at the interval of every 50 samples for sample calibration. A few of the measured soils contained inorganic carbon, which was removed from the sample by treated with diluted HCl before elemental analyses.

Soil aggregates were separated into two fractions (2–0.25 mm and <0.25 mm) by wet sieving (Six et al., 1998). Briefly, 10 g fresh soils (passed through 2 mm sieve) were placed on the top of 0.25 mm sieve, immersed in water-filled container for 5 min and then were gently oscillated for 20 min (4 cm amplitude, 25 cycles min^{-1}). The soils both remained on 0.25 mm sieve and passed through 0.25 mm were collected and freeze-dried. Organic carbon content of 2–0.25 mm aggregates was measured using an elemental analyzer (Elementar Vario EL Cube, Germany). The soil samples were treated with diluted HCl to remove the inorganic carbon prior to the determination. The proportion of organic carbon in 2–0.25 mm aggregates to bulk SOC was used to reflect SOC in macroaggregates.

After the reduction treatment of air-dried soils with a dithionite-citrate-bicarbonate solution, the residues were rinsed with deionized water for three times, freeze-dried, and then analyzed for SOC content with an elemental analyzer (Elementar Vario EL Cube, Germany) after treating with HCl. As a control treatment, soil samples were extracted with sodium chloride (NaCl). The oxides-bonded SOC content was calculated by subtracting SOC in control treatment from SOC in reduction treatment. The proportion of oxides-bonded SOC to bulk SOC was used to reflect SOC protected by soil oxides.

The chemical compositions of SOC were determined via cross polarization magic angle spinning solid-state ^{13}C-CPMAS NMR spectroscopy (Bruker Avance 300 spectrometer, Germany). Before analysis, air-

Table 2
Explanatory variables used to explain the variance of Q_{10} values.

Category	Variable Code	Variable description	Unit
R_f	R_f	Cumulative respired fraction	%
Climate	SoilT	Annual mean soil temperature	°C
	SoilTw	Average soil temperature in warmest month	°C
	SoilTc	Average soil temperature in coldest month	°C
	E	Elevation above sea level	m
Edaphic properties	pH	Soil pH	–
	SOCc	Soil organic carbon content	g kg^{-1}
	SOCs	Soil organic carbon stock	Mg ha^{-2}
	MBC	Microbial biomass content	mg kg^{-1}
	DOC	Dissolved organic carbon content	mg kg^{-1}
	DCN	The ratio of DOC to dissolved organic nitrogen	–
	SM	Soil moisture at the time of soil sampling	%
	TN	Total soil nitrogen content	g kg^{-1}
	TP	Total soil phosphorus content	g kg^{-1}
	POC	Particulate organic carbon content	g kg^{-1}
Physical protection	SC	The percentage of silt and clay	%
	FO	The sum of free oxides	mg kg^{-1}
	AO	The sum of amorphous oxides	mg kg^{-1}
	MOC	Mineral-associated organic carbon	g kg^{-1}
	MOC2	The proportion of MOC in total SOC	%
	MPOC	The ratio of MOC to POC	–
	OxiC	The proportion of oxides-bond C in total SOC	%
	AggC	The proportion of macroaggregate C in total SOC	%
	AFOC	The ratio of amorphous Fe/Al-bond C to SOC	–
	AFDC	The ratio of free Fe/Al-bond C to SOC	–
Molecular structure	AC	The proportion of alkyl C	%
	OAC	The proportion of O-alkyl C	%
	AROC	The proportion of aromatic C	%
	CARC	The proportion of carboxylic C	%
	ACOC	The ratio of alkyl C to O-alkyl C	–
	HBHI	The ratio of hydrophobic C to hydrophilic C	–
	PS	The proportion of polysaccharide C	%

Note: Except E, all variables were depth-specifically measured.

dried soil samples were treated with 10% HF (v/v) to remove paramagnetic materials. The treated samples were washed with deionized water, freeze-dried, and then sieved to pass a 0.149 mm screen. A semi-quantitative estimation of the main organic carbon functional groups was obtained by integrating four major chemical shift regions and the relative content of the different organic carbon functional groups were calculated as percentages of the area to the total spectrum area. The recorded ^{13}C spectra were quantified in the following chemical shift regions: alkyl C (0–45 ppm), O-alkyl C (45–110 ppm), aromatic C (110–160 ppm), and carbonyl/carboxyl C (160–220 ppm). O-alkyl C was separated into 45–60 ppm (methoxyl C), 60–90 ppm (C2–C6 carbohydrates) and 90–110 ppm (anomeric C). Aromatic C was divided into 110–145 ppm (aryl C) and 145–160 ppm (phenolic C). Three indexes were further calculated to reflect chemical recalcitrance of SOC (Li et al., 2017):

$$ACOC = \frac{alkyl\ C\ (0\text{-}45\ ppm)}{O\text{-}alkyl\ C\ (60\text{-}110\ ppm)} \quad (2)$$

$$HBHI = \frac{Hydrophobic\ C\ (0\text{-}45\ ppm + 110\text{-}160\ ppm)}{Hydrophilic\ C\ (60\text{-}110\ ppm + 160\text{-}220\ ppm)} \quad (3)$$

$$PolyC = 1.2 \times (O\text{-}alkyl\ C - phenolic\ C \times 1.5) \quad (4)$$

2.4. Soil incubation and estimation of Q_{10}

Soil samples (20 g fresh weight) were placed in 150-ml polyethylene plastic incubation bottles, which are designed for the automatic sampling and analysis system (Liu et al., 2017). After two weeks of pre-incubation at 20 °C to activate microorganisms and minimize the pulse effect, soils were incubated at designated temperatures of 5 and 15 °C with three replicates for a period of 128 days. During incubation, the bottles were sealed with caps that had small holes for ventilation and to reduce water loss, and soil moisture in all bottles was maintained at 60% of water-holding capacity by repeatedly weighing and adjusting water. The mineralization rate of SOC (R_s) was measured 13 times using an automatic temperature control soil flux system (PRI-8800; Pri-Eco, Beijing, China) as described in He et al. (2013). We calculated R_s for day 1, 2, 4, 6, 9, 16, 23, 37, 51, 65, 86, 107 and 128 of the incubation. The system samples and measures R_s at programmed time intervals automatically. On each measurement date, daily R_s (μg CO_2–C g^{-1} SOC day^{-1}) were normalized to per unit SOC. The cumulative carbon mineralization (R_{cum}, μg CO_2–C g^{-1} SOC) during the incubation period was linearly interpolated using R_s. Based on R_{cum} at the end of the incubation, we calculated Q_{10} ($Q_{10\text{-}cum}$) as:

$$Q_{10-cum} = \left(\frac{R_w}{R_c}\right)^{\frac{10}{T_w - T_c}}, \quad (5)$$

where R_w and R_c are the cumulative mineralization of SOC (μg CO_2–C g^{-1} SOC) under warm (T_w, i.e., 15 °C) and cold (T_c, i.e., 5 °C) temperatures, respectively.

In addition, Q_{10} values for different cumulative respired fractions of SOC decomposition were calculated using $Q_{10\text{-}q}$ method (Conant et al., 2008). Q_{10} based on this fraction was estimated as:

$$Q_{10-q} = \left(\frac{t_c}{t_w}\right)^{\frac{10}{T_w - T_c}}, \quad (6)$$

where t_c and t_w are the time needed to respire a given fraction of SOC at T_c and T_w, respectively. Considering the continuum nature of SOC lability, the fraction of respired SOC was determined at continuous gradients with an interval of percentage respired SOC of 0.1% (i.e., 0–0.1%, 0.1–0.2%, 0.2–0.3%, …, which represent a gradient of decreasing lability of SOC with the decomposition of SOC acknowledging that labile fractions decompose fast). For all incubated soils, we calculated $Q_{10\text{-}q}$ for all respired fractions at the interval of 0.1%. Depending on the incubation temperature and soil sample, the maximum respired fraction ranges from 0.3% to 1.3%.

2.5. Modelling carbon pools and their Q_{10}

Using measurements of R_s, we fitted a three-pool model to derive Q_{10} for each pool:

$$R_t = k_f \cdot C_f \cdot e^{-k_f \cdot t} + k_s \cdot C_s \cdot e^{-k_s \cdot t} + k_p \cdot C_p \cdot e^{-k_p \cdot t}, \quad (7)$$

where $C_f = f_f \cdot C_0$, $C_s = f_s \cdot C_0$, $C_p = f_p \cdot C_0$, $f_f + f_s + f_p = 1$, R_t is the SOC mineralization rate at day t (μg CO_2–C g^{-1} SOC day^{-1}); f_f, f_s and f_p are the fraction of fast, slow (C_s) and passive pool (C_p) in total SOC at the start of the incubation (C_0), respectively, with decay rate of k_f, k_s and k_p (day^{-1}), respectively. In this study, we designed a new model configuring procedure considering the relatively short-term period of the incubation. First, we pre-defined decay rates of 0.2 (which is equivalent to a turnover time of 5 days, k_f) under 15 °C for the fast C pools, and 0.02 day^{-1} (which is equivalent to a turnover time of 50 days, k_s) for slow C pools. Then, using the mineralization data under 15 °C, the pool size of the two pools were optimized. For the passive pool, we assume that its

turnover time is much longer than the duration of the incubation, and both its decay rate and size were optimized. Under 5 °C incubation, the model shared the optimized pool sizes under 15 °C, but their decay rates were re-optimized. That is, the three pools are defined by certain decay rates under 15 °C, and incubation temperature only changes the decay rates rather than the size of a C pool. This approach with pre-defined decay rates has an advantage of making the pools (particularly the fast and slow pools) comparable across sites and through soil depths.

Model parameters were optimized using Bayes' theorem. The sum of the probability density of predictions (θ) was maximized to target the best agreement between predictions and observations:

$$\theta = \sum_{i=1}^{n} \frac{1}{\sqrt{2 \cdot \pi \cdot \sigma_i^2}} \cdot e^{-\frac{(x_i - \mu_i)^2}{2 \cdot \sigma_i^2}}, \quad (8)$$

where μ_i is the average of ith observations of R_s, σ_i the standard deviation of the replicates of the ith observations, x_i the corresponding model predictions, n the total sample size of observations ($n = 13$). For k_p, we assumed a prior uniform distribution ranging from 1e-5 (which is equivalent to a turnover time of ~274 years) to k_s. For f_f, f_s and f_p, a prior uniform distribution was assumed (0–0.1 for f_f and 0–0.2 for f_s, acknowledging that the two labile pools may only account for a small fraction of total SOC), given the condition: $f_f + f_s + f_p = 1$. The initial fractions of the three pools of the same soil were shared by both incubation temperatures considering that incubation temperature does not change this fraction. Posterior probability distributions of parameters were obtained using the differential evolution adaptive metropolis algorithm (Vrugt and Ter Braak, 2011) – a Markov Chain Monte Carlo (MCMC) technique – by running three chains. Gelman–Rubin diagnostic index (G) was used to determine the convergence of the MCMC simulations (Brooks and Gelman, 1998) with a threshold value of 1.01. That is, if G is less than 1.01 for all parameters, the MCMC simulations were considered to be converged. Using the optimized model parameters, the model could explain 98% of the variance of R_s (Fig. S1). The MCMC was run using the *runMCMC* function in package *BayesianTools* in R version 4.0.3 (R Development Core Team, 2021). Using the optimized decay rates (i.e., k_f, k_s and k_p) for each pool, we calculated Q_{10} values for each pool as (Qin et al., 2019):

$$Q_{10-k} = \left(\frac{k_w}{k_c}\right)^{\frac{10}{T_w - T_c}}, \quad (9)$$

where k_w and k_c are the optimized decay rates of a pool under T_w and T_c, respectively.

2.6. Statistical analyses

For $Q_{10\text{-cum}}$, we examined its difference among soil depths (D, i.e., the five depths with three replicates for each depth) and elevations (E, i.e., the ten elevations) using a two-way analysis of variance (ANOVA) with the consideration of possible interactions. For $Q_{10\text{-k}}$ and $Q_{10\text{-q}}$, a three-way ANOVA was conducted by including the modeled three SOC pools (P) and respired SOC fractions (R_f) as another variable, respectively. Data normality and variance homoscedasticity were tested using the Shapiro-Wilk test and Levene's test, respectively. When normality or variance homoscedasticity were not achieved, data were log-transformed. Focusing on $Q_{10\text{-cum}}$, a correlation analysis was conducted to assess its correlation with elevation, depth and the measured edaphic properties and SOC compounds. A canonical ordination-based redundancy analysis (RDA) (Borcard et al., 2011) was also conducted to explicitly explore the relationships between Q_{10} metrics (i.e., $Q_{10\text{-cum}}$, $Q_{10\text{-q}}$, $Q_{10\text{-k}}$) and an explanatory matrix. The explanatory matrix includes a suite of variables reflecting climatic and edaphic conditions as well as measurements reflecting SOC physiochemical stability (Table 2). The RDA was performed on standardized Q_{10} values and explanatory variables using the *rda* function in R package *vegan*.

Focusing on $Q_{10\text{-q}}$ values we further conducted a machine learning-based random forest analysis (RFA) (Haaf et al., 2021) to identify the main predictors of Q_{10} to complement RDA results. We classified the predictor variables into six groups: 1) climate conditions indicated by elevation and soil temperature, 2) edaphic properties (e.g., soil pH, soil moisture, SOC), 3) physiochemical protection of SOC (e.g., MOC, macroaggregate occluded-C, Fe/Al-bound C), 4) molecular structure of SOC determined by ^{13}C CP-MAS NMR, 5) respired fraction (R_f, which represents the lability of respired SOC) and 6) soil depth. The relative importance of individual variables for the six groups of predictors were summed respectively to indicate their overall relative importance. These analyses were conducted using the *randomForest* package in R version 4.0.3 (http://cran.r-project.org/). In addition, we used path analysis (i.e., structural equation models) to further clarify the complex interconnections among predictors. The abovementioned variable groups (e.g., climate conditions, edaphic properties, physical protection, and molecular structure) were included as latent variables in the path analysis. Fig. S2 shows the individual indicators for each latent variable. The partial least squares (PLS) approach was used for the path analysis (PLS-PA). A non-parametric bootstrapping (200 resamples in this study) was used to estimate the precision of the PLS parameter estimates. The 95% bootstrap confidence interval was used to judge that whether the estimated path coefficients are significant. All predictors in the PLA-PA were standardized. The PLS-PA analyses were performed using the package *plspm* in R version 4.0.3 (http://cran.r-project.org/).

3. Results

$Q_{10\text{-cum}}$ values varied widely across the ten elevations and five soil depths, ranging from 1.61 to 2.24 (Fig. 1a). This variation of $Q_{10\text{-cum}}$ was predominantly explained by elevation ($F = 45.72$, $p < 0.001$), while the effect of depth was relatively weak albeit significant ($F = 6.93$, $p < 0.001$; Table 3, Fig. 1a). Correlation analysis also suggested that Q10-cum was more strongly correlated to elevation than to soil depth (Fig. 2a vs 2b). For $Q_{10\text{-q}}$ estimated for three respired fractions of 0–0.1%, 0.2–0.3%, and 0.4–0.5%, which represents substrate lability, its variance was also mainly influenced by elevation ($F = 53.30$, $p < 0.001$; Table 3). It was also apparent that $Q_{10\text{-q}}$ significantly increased with decomposition (Fig. 1b, c, d). Specifically, for R_f of 0–0.1%, $Q_{10\text{-q}}$ on average was 2.42 across the elevations and depths, it was increased to 2.44 for R_f of 0.2–0.3% and 2.52 for R_f of 0.4–0.5% (Fig. 1b, c, d). Besides $Q_{10\text{-cum}}$ and $Q_{10\text{-q}}$, modelling based on the three-pool C model found that passive pool (C_p, average $Q_{10\text{-q}} = 3.83$) had significantly higher $Q_{10\text{-k}}$ than fast pool (C_f, average $Q_{10\text{-q}} = 3.35$) and slow pool (C_s, average $Q_{10\text{-q}} = 2.82$) (Fig. 1e, f, g). Three-way ANOVA again identified that the effect of three pools themselves on the variance of Q_{10} was significantly higher than elevation and soil depth (Table 3). These results demonstrated the vital role of soil elevation-origin and SOC lability (which is reflected by both the cumulative respired fractions and three modeled SOC pools) in controlling temperature sensitivity of soil SOC mineralization.

In terms of the chemical composition of SOC, both ACOC and HBHI were increased with soil depth and elevation (Fig. 3a, b, c). More recalcitrant SOC in deeper depth of colder regions was observed. Correlation analysis showed that Q_{10} was significantly ($P < 0.001$) and positively correlated with ACOC and HBHI at all soil depths (Fig. 4). MOC2, OxiC and AggC were also significant correlated to soil depth and elevation (Fig. 3d, e, f). Specifically, the proportion of mineral-associated and oxides-bounded SOC were increased with soil depth, whereas less proportion of SOC was occluded within macroaggregates (2–0.25 mm) in deep soil layers. Besides, more SOC was protected by soil aggregates and oxides in higher elevation soils (Fig. 3f).

The RDA explained 73% (i.e., $R^2 = 0.73$) of the total variance of the data (Fig. 5), to which the first two canonical axes (i.e., RDA 1 and RDA 2) contributed 59% and 14%, respectively (Fig. 5). This result demonstrated that the major linear trends/relationships in the data had been

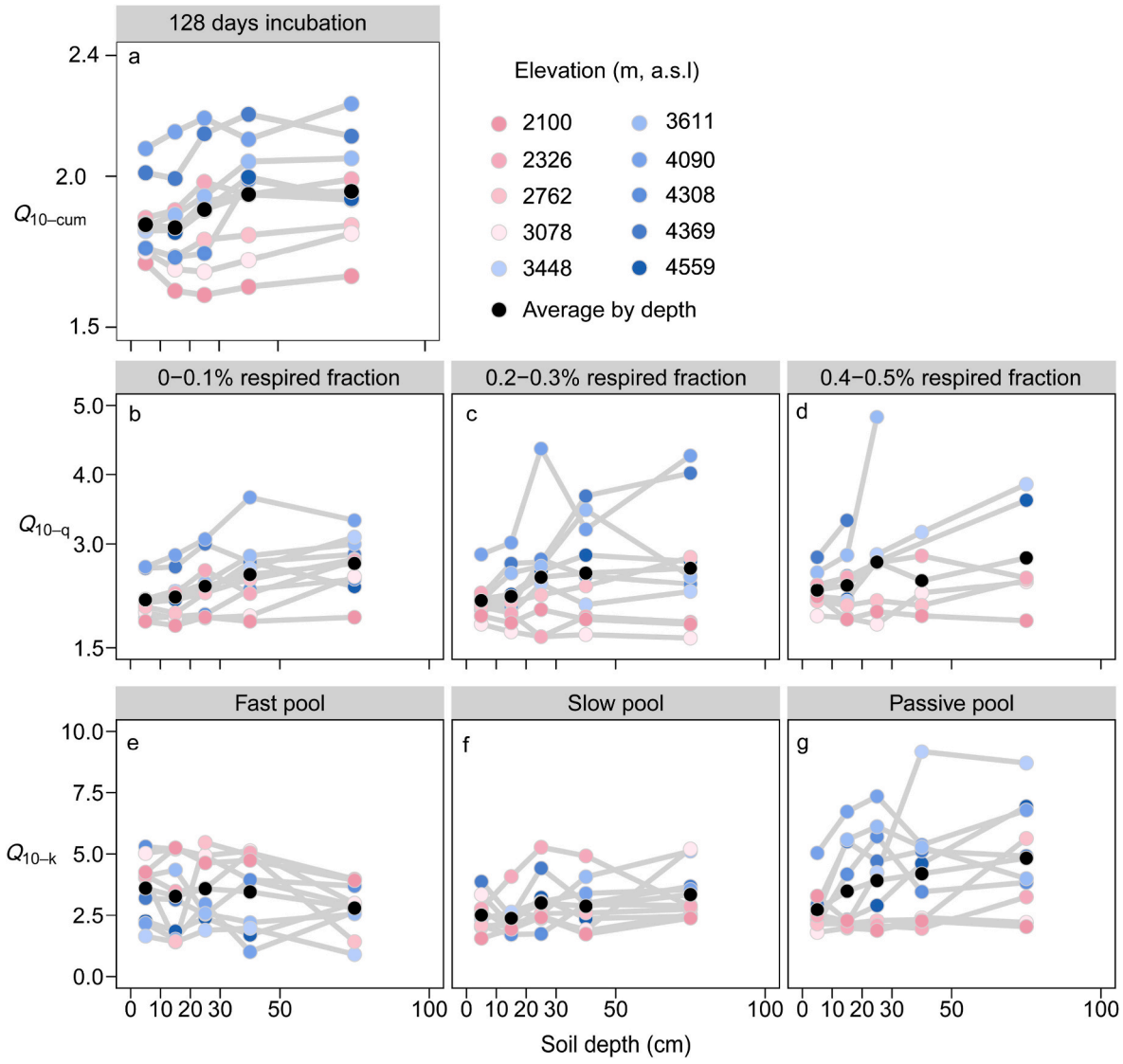

Fig. 1. Variation of Q_{10} values across soil depths and elevations. $Q_{10\text{-cum}}$, calculated based on cumulative respiration at the end of the 128-day incubation; $Q_{10\text{-q}}$, calculated for cumulative respired fractions of 0–0.1%, 0.2–0.3% and 0.4–0.5% using the $Q_{10\text{-q}}$ method; $Q_{10\text{-k}}$, calculated based on the decay rates of three pools (i.e., fast, slow and passive pools) modeled by a three-pool carbon model. Points at elevations of 4559, 4090, 3448, 2762, 2070 m are average values of three replicates. See Table 3 for statistics of analysis of variance of Q_{10} values.

captured by the RDA and could well explain the data. Among the 30 potential controlling factors assessed (Table 2), 16 of them were identified to have significant effects. Specifically, HBHI, ACOC, AC, OxiC played an important role in RDA 1 and were positively correlated to each other (the angle between these variables were less than 90°, Fig. 5). Three variables representing depth-specific soil temperature along the elevation transect (i.e., SoilT, SoilTw and SoilTc) were important for both RDA 1 and 2. MPOC was also important for RDA 2. Both $Q_{10\text{-cum}}$ and $Q_{10\text{-q}}$ were apparently positively correlated to HBHI, ACOC, AC, OxiC, SC, TP, SOCs and MPOC, but negatively correlated to SoilT, SoilTw, SoilTc and pH (the angle between these variables and $Q_{10\text{-cum}}$ and $Q_{10\text{-q}}$ were larger than 90°, Fig. 5). It is intriguing to note that $Q_{10\text{-k}}$ for the three pools (i.e., $Q_{10\text{-fast}}$, $Q_{10\text{-slow}}$ and $Q_{10\text{-passive}}$) simulated by the three-pool carbon model presented distinct relationships with explanatory variables (Fig. 5). For example, $Q_{10\text{-fast}}$ was positively correlated to soil temperature and negatively correlated to AO, but $Q_{10\text{-passive}}$ showed opposite correlations to these variables (Fig. 5). This result highlighted that temperature sensitivity of pools with different decay rates is determined by distinct processes (i.e., chemical recalcitrance and physiochemical stabilization).

As expected, random forest analysis, which considers non-linear relationships, explained more ($R^2 = 0.85$) variance of $Q_{10\text{-q}}$ with a RMSE of 0.21 (Fig. 6a) compared with RDA (Fig. 5). In line with the RDA result, HBHI (i.e., the ratio of hydrophobic to hydrophilic carbon substrates) was the most important predictor variable which alone contributed 22% to the explained variance among the ten most important controlling factors (Fig. 6b). Following HBHI, R_f (cumulative respired fraction) and ACOC (the ratio of alkyl C to O-alkyl C) were the two most important, and each contributed another >10% (Fig. 6b). Grouping the explanatory variables into six groups reflecting chemical molecular structure, physical protection, respired fraction, edaphic properties, climatic conditions and soil depth, the results showed that the three groups relating to chemical composition and physiochemical stabilization of SOC (i.e., molecular structure, physical protection and respired fraction) contributed >80% of the explained variance (Fig. 6b). Similar to RDA results, partial dependence analysis indicated that $Q_{10\text{-q}}$ was generally positively correlated to HBHI, RF, ACOC, AFOC, AC, OAC, but negatively to AFDC, OxiC, SoilTc and PS (Fig. 6c). However, it should be noted that there was high variability in the controlling factors for $Q_{10\text{-q}}$, demonstrating nonlinear relationships between Q_{10} and controlling

Table 3
Analysis of variance of temperature sensitivity of soil organic carbon (SOC) decomposition estimated by different Q_{10} approaches as impacted by different controlling factors.

Q_{10}	Variables	*df*	*F*	*p*
$Q_{10\text{-cum}}$	Elevation (E)	9	45.72	***
	Soil depth (D)	4	6.93	***
	E × D	36	0.78	ns
$Q_{10\text{-q}}$	E	9	53.30	***
	D	4	26.73	***
	Respired fraction (R_f)	12	5.78	***
	E × D	36	3.41	***
	E × R_f	48	2.39	***
	D × R_f	39	0.89	ns
	E × D × R_f	147	0.98	ns
$Q_{10\text{-k}}$	E	9	2.04	*
	D	4	3.03	*
	SOC pool (P)	2	68.93	***
	E × D	36	1.07	ns
	E × P	18	12.89	***
	D × P	8	2.98	**
	E × D × P	72	1.95	***

Note: ns, non-significant; *, $p < 0.05$; **, $p < 0.01$; ***, $p < 0.001$.

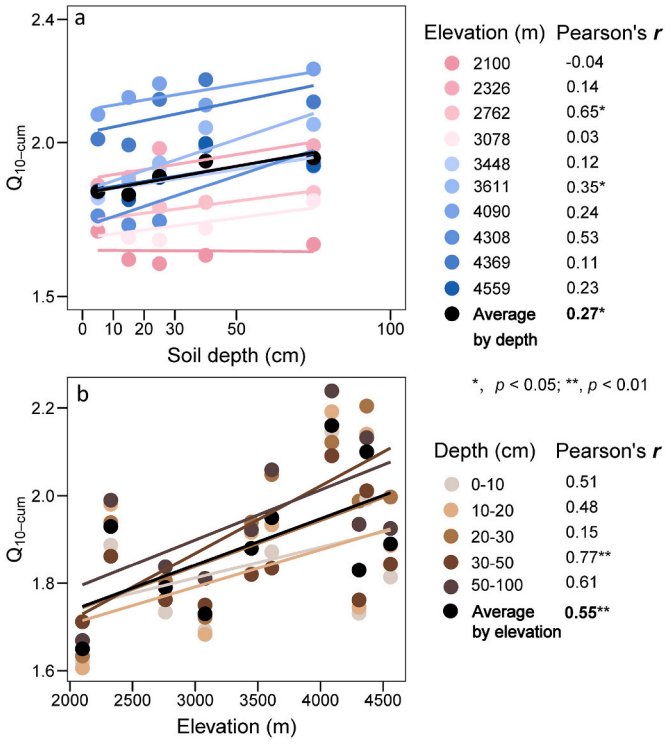

Fig. 2. The correlation of $Q_{10\text{-cum}}$ with soil depth and elevation. $Q_{10\text{-cum}}$, calculated based on cumulative respiration at the end of the 128-day incubation.

factors (Fig. 6c).

The path analysis considering the direct and indirect effects of climate, soil depth, edaphic properties, molecular structure, and physical protection could explain 63%, 50%, 42%, 31% and 70% of the variance of $Q_{10\text{-cum}}$, $Q_{10\text{-q}}$, $Q_{10\text{-fast}}$, $Q_{10\text{-slow}}$ and $Q_{10\text{-passive}}$, respectively (Fig. 7). For $Q_{10\text{-cum}}$, molecular structure and physiochemical protection presented the strong direct effect (the path coefficient reaches to 0.77 and 0.45, respectively), while the direct effects of other variables were relatively weak and insignificant (Fig. 7b). However, the effects of climate (e.g., Elevation and SoilT) and edaphic properties (i.e., pH, SM, SOC, TP and TN) manifested via its effect on physical protection (indirect effect), while 78% of the variance of physical protection could be explained by these variables (Figs. 7b and 6 and S2). Particularly, climate showed the strongest indirect effect on $Q_{10\text{-cum}}$ and even exceeded the direct effect of physical protection (Fig. 8). As the distinct controlling factors for Q_{10} of the three modeled pools identified by the RDA (Fig. 5), the path analysis also found that $Q_{10\text{-fast}}$ was predominantly influenced by physical protection and, to a less extent, by climate; while the direction of the effect of climate on $Q_{10\text{-slow}}$ and the direction of the effect of molecular structure on $Q_{10\text{-passive}}$ were the same, the direction of the effect of edaphic properties on $Q_{10\text{-slow}}$ and $Q_{10\text{-passive}}$ was reversed (Fig. 7b). Generally, physical protection and/or molecular structure exerted the strongest direct effects, while the indirect effects of climate manifested via its marked effects on physical protection and molecular structure (Figs. 7 and 8). Above all, these results revealed the dominant role of molecular structure and/or physical protection in regulating Q_{10} which in turn was predominantly regulated by climatic conditions reflected by elevation and soil profile temperature (Figs. 7 and 8 and S2).

4. Discussion

4.1. Q_{10} variation across soil depths

In the study region, we found that soil depth has significant effect on temperature sensitivity of SOC decomposition, but this effect is relatively small compared with the effect of elevation (Table 3, Figs. 1 and 2). Across the elevational transect from 3365 to 4590 m in the same study region, Xu et al. (2021) found that Q_{10} of SOC decomposition at two depths (0–20 cm vs 40–60 cm) ranged from 1.28 to 2.10 by incubating soil samples for 60 days. These Q_{10} values are in line with our Q_{10} estimates in the similar elevation range of Sygera mountains. In the literature, there are contradictory conclusions on the temperature sensitivity of SOC decomposition across soil depths, which may be a consequence of contrasting climatic, edaphic and biological conditions (e.g., vegetation cover) and method applied among the studies (Li et al., 2018, 2020; Qin et al., 2019; Vaughn and Torn, 2019; Xu et al., 2021). The short-term (hours to days) temperature sensitivity of SOC decomposition of 90 upland forests soils, as examined using a dynamic temperature ramping method, was reported to significantly increase with soil depth (Li et al., 2020). On the contrary, a 330-day incubation of permafrost soils from Tibet, China, detected weaker temperature sensitivity of SOC in deeper layers due to lower substrate accessibility for microbial decomposition (Qin et al., 2019). In a temperate forest, in situ warming of soil profile down to 1 m found that soil respiration to warming did not show significant difference among soil depths, albeit heterotrophic respiration derived from SOC mineralization was not separated from the total soil respiration (Hicks Pries et al., 2017). Our results here showed that Q_{10} increased with soil depth, particularly in higher elevation gradients (e.g., from elevation 3411 m–4559 m; Fig. 1). As indicators for physiochemical protection of SOC (e.g., MOC, OxiC and AggC) exhibited similar variation with soil depth among the ten sampling sites (Fig. 3), the greater depth-induced increase in Q_{10} in higher elevational soils might be attributed to more recalcitrant SOC in deep soils. Based on these results, under future climate warming, our results provide additional evidence that SOC in different soil layers may show variable response to warming under different climatic and edaphic conditions. Mechanisms underpinning such spatial variability should be further elucidated.

4.2. Q_{10} variation across elevations

Among vegetations distributed along the 2500 m elevation transect, significant difference in Q_{10} was observed. It was general that SOC in higher elevations was more sensitive to temperature changes (Figs. 1 and 2). This result derived from the temperature gradient along the elevation transect is well in line with findings based on data synthesizing and process-based modelling across large spatial extents covering

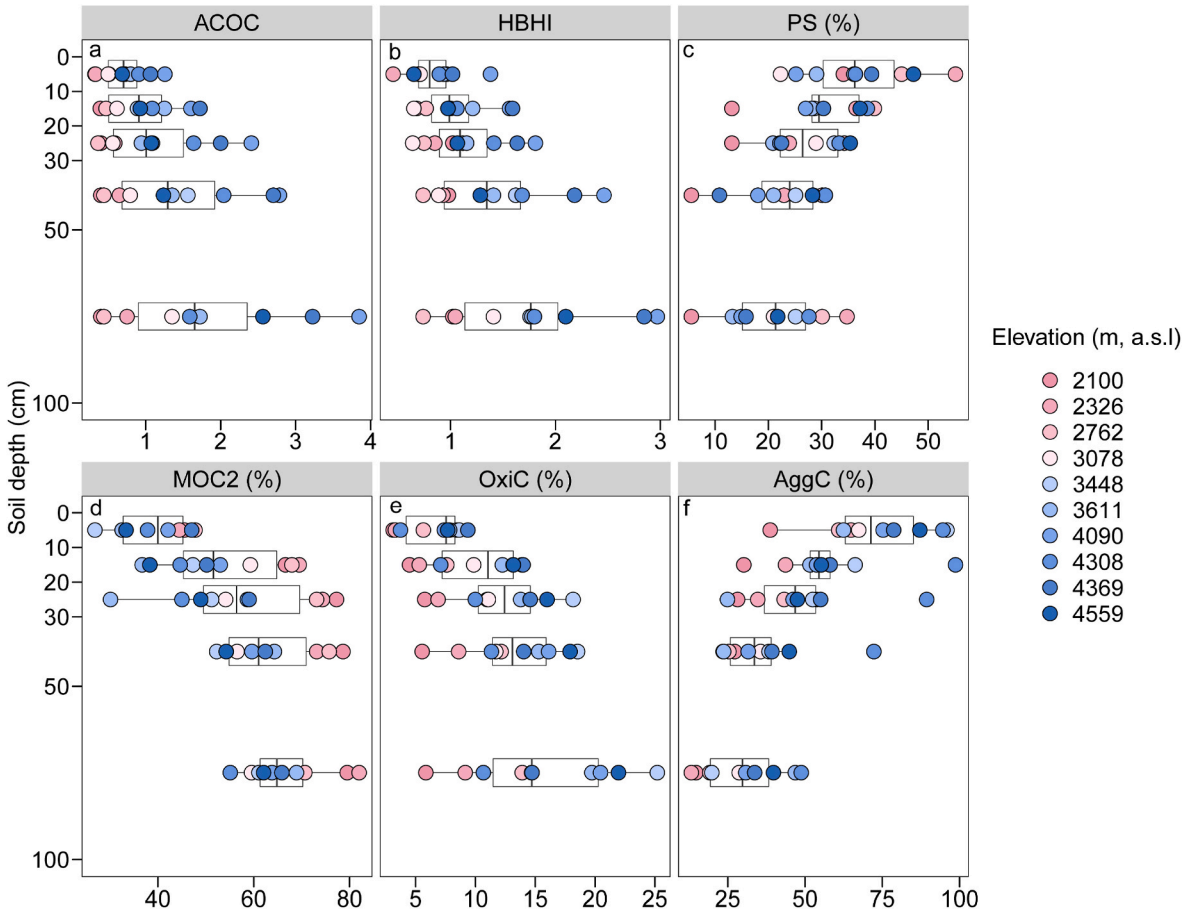

Fig. 3. Chemical composition (a–c) and physiochemical protection indicators (d–f) of SOC across soil depths and elevations. ACOC, the ratio of alkyl C to O-alkyl C as investigated by ^{13}C-NMR; HBHI, the ratio of hydrophobic C to hydrophilic C as investigated by ^{13}C-NMR; PS, the proportion of polysaccharide C as investigated by ^{13}C-NMR; MOC2, the proportion of MOC in total SOC; OxiC, the proportion of oxides-bond C in total SOC; AggC, the proportion of macroaggregate C in total SOC.

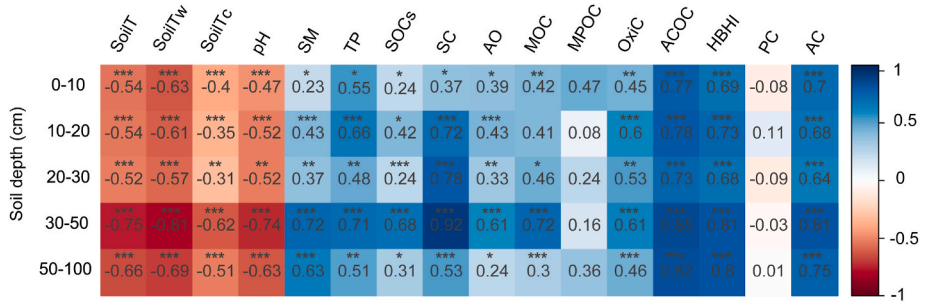

Fig. 4. Correlation coefficients (pearson's r) between $Q_{10\text{-cum}}$ and examined variables in each soil depth. *, $p < 0.05$; **, $p < 0.01$; ***, $p < 0.0001$. See Table 2 for explanation of the abbreviations.

diverse climate zones (Koven et al., 2017; Wang et al., 2019; Lei et al., 2021). That is, SOC decomposition is more sensitive to temperature changes in colder regions. There would be two aspects of reasons underpinning such climate-driven temperature sensitivity of SOC decomposition: the composition of SOC and vegetation. In terms of SOC composition, in cold regions, plant materials decompose slowly due to low temperature, resulting in a high proportion of particulate organic carbon in total SOC (Mueller et al., 2015; Poeplau et al., 2017), while particulate organic carbon has been found to be more sensitive to temperature compared with other pools such as mineral-associated organic carbon (Lugato et al., 2021). Besides, vegetation (e.g., forest vs grassland) under different climatic conditions have distinct litter production in terms of quantity and quality as well as root dynamics (Freschet et al., 2017; Wang et al., 2019), which ultimately influence SOC formation and transformation thereby its temperature sensitivity (Wagai et al., 2013; Cordova et al., 2018). Regression analysis (Fig. 4) revealed that Q_{10} was more related to depth-specific soil temperature (negative coefficients) and SOC chemical composition (positive coefficients) across sites in all soil depths. Our data also showed that the chemical composition of SOC (e.g., AC – the proportion of alkyl C estimated from ^{13}C-NMR peak areas) is closely correlated to soil climate as reflected by mean annual soil temperature and mean soil temperature in warmest month (Fig. 5). Above all, it is reasonable to propose that climate-induced shifts vegetation cover that control carbon inputs (in terms of both quality and quantity) might be the underlying reasons of climatological control on Q_{10}.

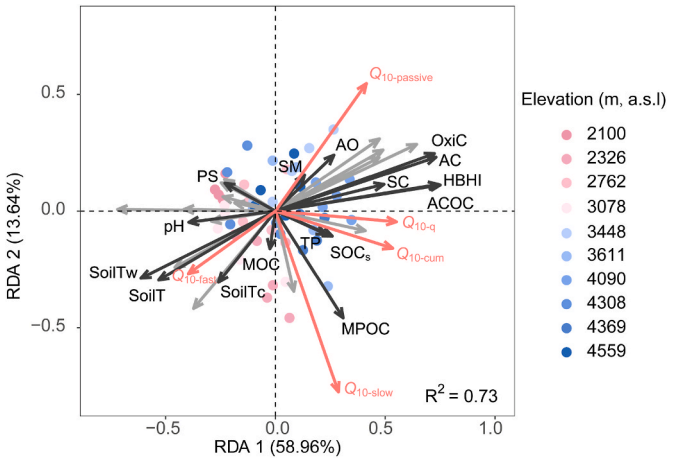

Fig. 5. Redundancy analysis demonstrating the correlations of Q_{10} values to a series of variables. The first and second RDA axes can explain 59% and 14% of variances of the Q_{10} metrics. Insignificant variables are in grey color. See Table 2 for explanation of the abbreviations. (For interpretation of the references to color in this figure legend, the reader is referred to the Web version of this article.)

4.3. Q_{10} as impacted by chemical composition and physical protection of SOC

Our multi-approach assessment provided evidences that both chemical composition of SOC represented by molecular structure and physiochemical carbon pools were identified to be important for Q_{10} (Figs. 5–7). Specifically, for $Q_{10\text{-cum}}$ and $Q_{10\text{-q}}$ (which are two metrics representing overall temperature sensitivity of SOC decomposition), molecular structure and physiochemical protection presented strong direct effects (the path coefficient reaches to 0.77 and 0.45 for $Q_{10\text{-cum}}$, and 0.63 and 0.54 for $Q_{10\text{-q}}$, respectively), while the direct effects of other variables were relatively weak (Fig. 7). In addition, the RFA results also demonstrated that Q_{10} variations were primarily explained (41.08%) by molecular structure, and followed by physical protection (28.24%, Fig. 6b). It is generally accepted that more chemically recalcitrant compounds have a higher intrinsic temperature sensitivity (Davidson and Janssens, 2006). As the Q_{10} values in this study were apparent temperature sensitivity, our result indicated that the intrinsic sensitivity does not vanish albeit the divergent soil and climate conditions along the elevation transect and through soil profile. Indeed, the comprehensive measurements of SOC composition relating to physiochemical protection of SOC against decomposition (i.e., accessibility of SOC to microbial decomposition) enabled us to distinguish the effect of chemical recalcitrance and accessibility. The results found that while chemical composition of SOC governed Q_{10}, physiochemical protection of SOC was found to be also important, demonstrating that the temperature sensitivity of SOC decomposition is modulated by combined, integrated effects of both chemical recalcitrance and physiochemical protection.

According to the calculation of cumulative respired C fraction (Rf), it is noteworthy that $Q_{10\text{-q}}$ significantly increases with Rf (Fig. 1b, c, and d). Rf represents a gradient of decreasing lability of SOC with the proceeding of incubation. This decrease of lability would be due to the reduce of chemically labile substrates (e.g., microbes would preferentially use this C fraction) (Nottingham et al., 2019) and/or increase of environmental constraints on SOC decomposition (e.g., soil compaction and acidification with the proceeding of incubation). There is evidence that SOC turnover is more strongly controlled by carbon accessibility rather than carbon recalcitrance (Dungait et al., 2012; Hemingway et al., 2019; Qin et al., 2019). In terms of SOC dynamics in response to global warming, our results suggest that both chemical recalcitrance and accessibility are important. As such, SOC pools with distinct physiochemical properties would exert different temperature sensitivities. Indeed, this expectation has been supported by the results based on the three-pool model which divide SOC to fast, slow and passive pools. The redundancy analysis showed that $Q_{10\text{-fast}}$ was positively correlated to soil temperature, while the $Q_{10\text{-passive}}$ showed opposite correlations to these variables and were more related to the variables reflecting the molecular composition and physiochemical protection of SOC (Fig. 5). These results indicated that potential mechanisms regulating Q_{10} differed for various soil C pools. To be specific, most organic compounds in fast C pool are mainly unprotected and readily accessibility to soil microbes (Schmidt et al., 2011). As such, Q_{10} variation in this C pool was primarily mediated by microbial communities (Qin et al., 2019), while the diversity and composition of microbial community shifted with climatic gradients (Djukic et al., 2010; Xu et al., 2021). However, as the proceeding of decomposition and exhausting of labile C pool, the quality of substrates and SOC protection against decomposition become the major determinants of Q_{10}.

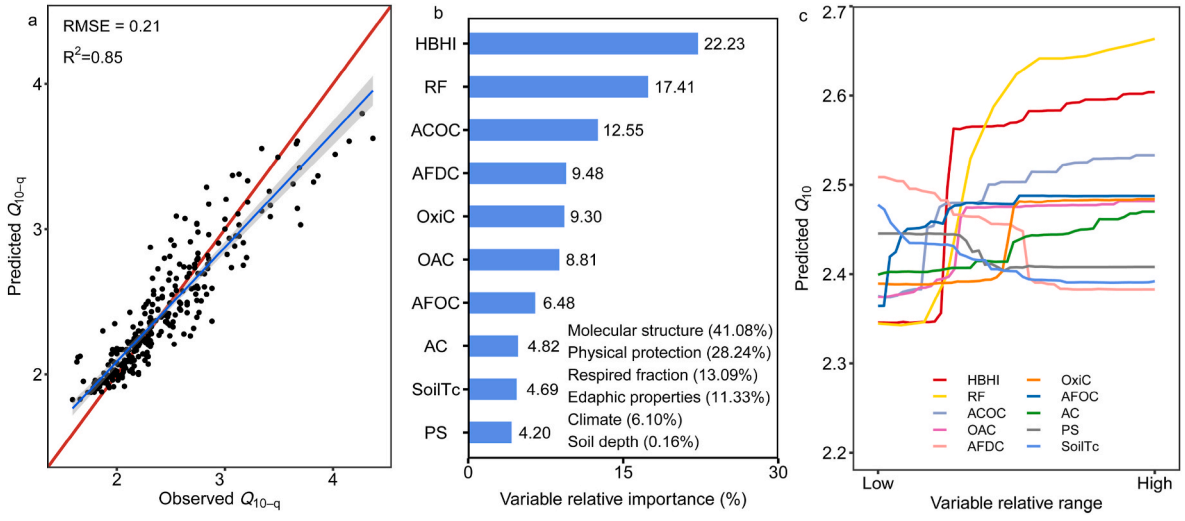

Fig. 6. Model performance and controlling factors of $Q_{10\text{-q}}$ values. a, the performance of a random forest model to explain the variance of $Q_{10\text{-q}}$ values across soil depths and elevations. RMSE, rooted mean squared error; R^2, the determinant coefficient of model. **b**, the ten most important controlling factors identified by the random forest model and their contribution to the explained variance. **c**, partial dependence of $Q_{10\text{-q}}$ values on the identified ten factors. See Table 2 for explanation of abbreviations of the variable predictors.

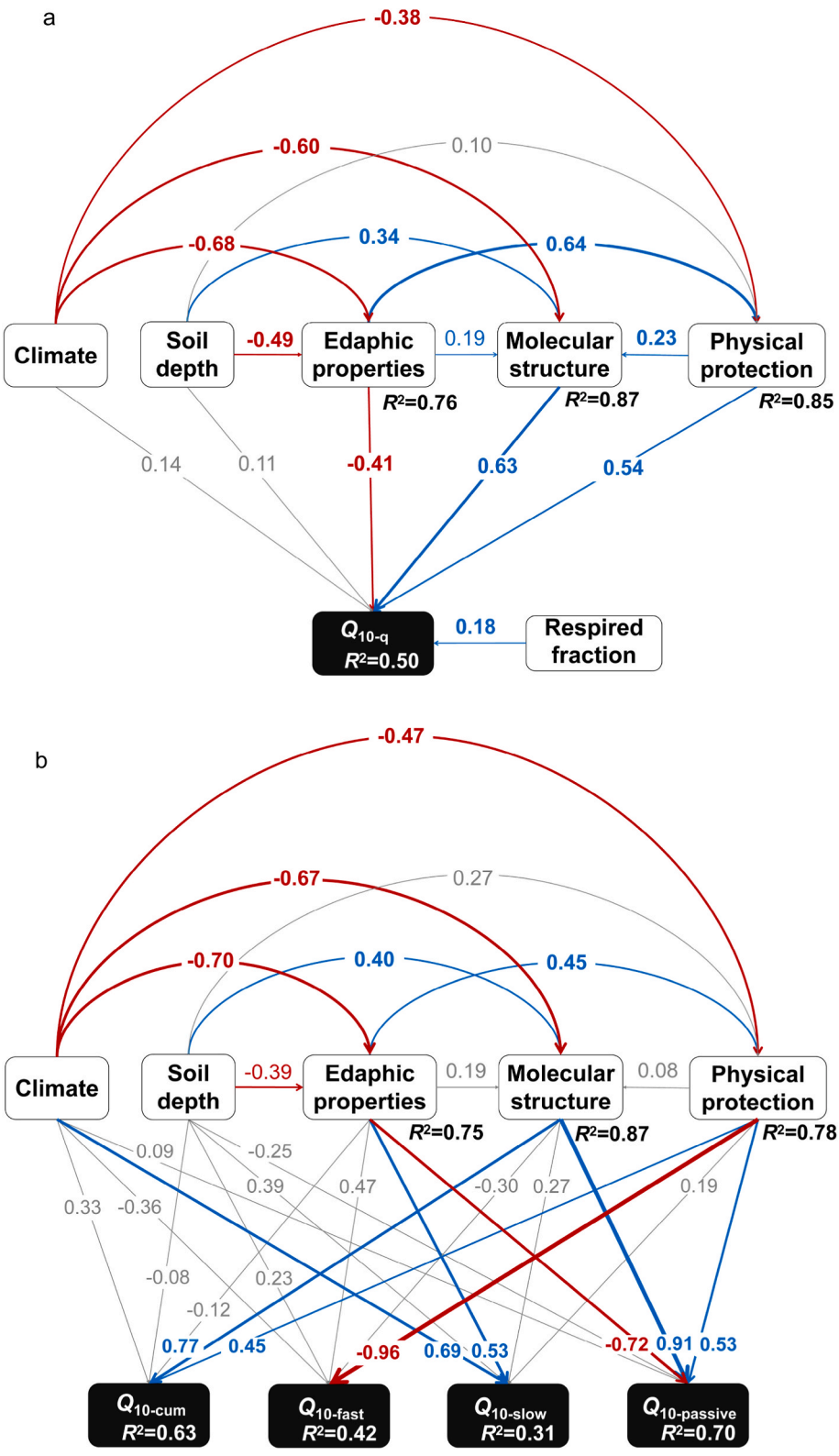

Fig. 7. Path analysis results of the controlling factors on Q_{10}. Numbers show the path coefficients. Arrows indicate the effect direction, while red and blue paths indicate the effect is significantly ($p < 0.05$) negative and positive, respectively, and the magnitude of path coefficients are represented by the path thickness. Insignificant paths are shown as grey lines. Indicators for the relevant latent variable are shown in Table 2, and the loadings of individual variables to the latent variables are shown in Fig. S2. R^2 shows the determinant coefficient for the corresponding variable, indicating the variance explained by the model. (For interpretation of the references to color in this figure legend, the reader is referred to the Web version of this article.)

The results further revealed that the direct effect of climate of Q_{10} was small, but climate could explain ~80% of the variance of chemical composition and physiochemical protection of SOC (Figs. 7 and 8). As such, the influence of climate was mainly indirectly reflected via its predominant effect on chemical composition and physiochemical protection, directly supporting our previous proposition. As been discussed above, climate is the predominant factor determining: 1) vegetation type therefore chemistry and quality of carbon inputs to soil (Coûteaux et al., 1995; Aerts, 1997), 2) soil pedogenesis process therefore organo-mineral interactions or/and aggregate protection (Doetterl et al., 2015, 2018), and 3) microbial community composition and functioning therefore the quantity and quality of microbial necromass which is considered to be resistant to decomposition and a significant contributor to the soil C pool (Liang et al., 2019; Wang et al., 2021). In the context of

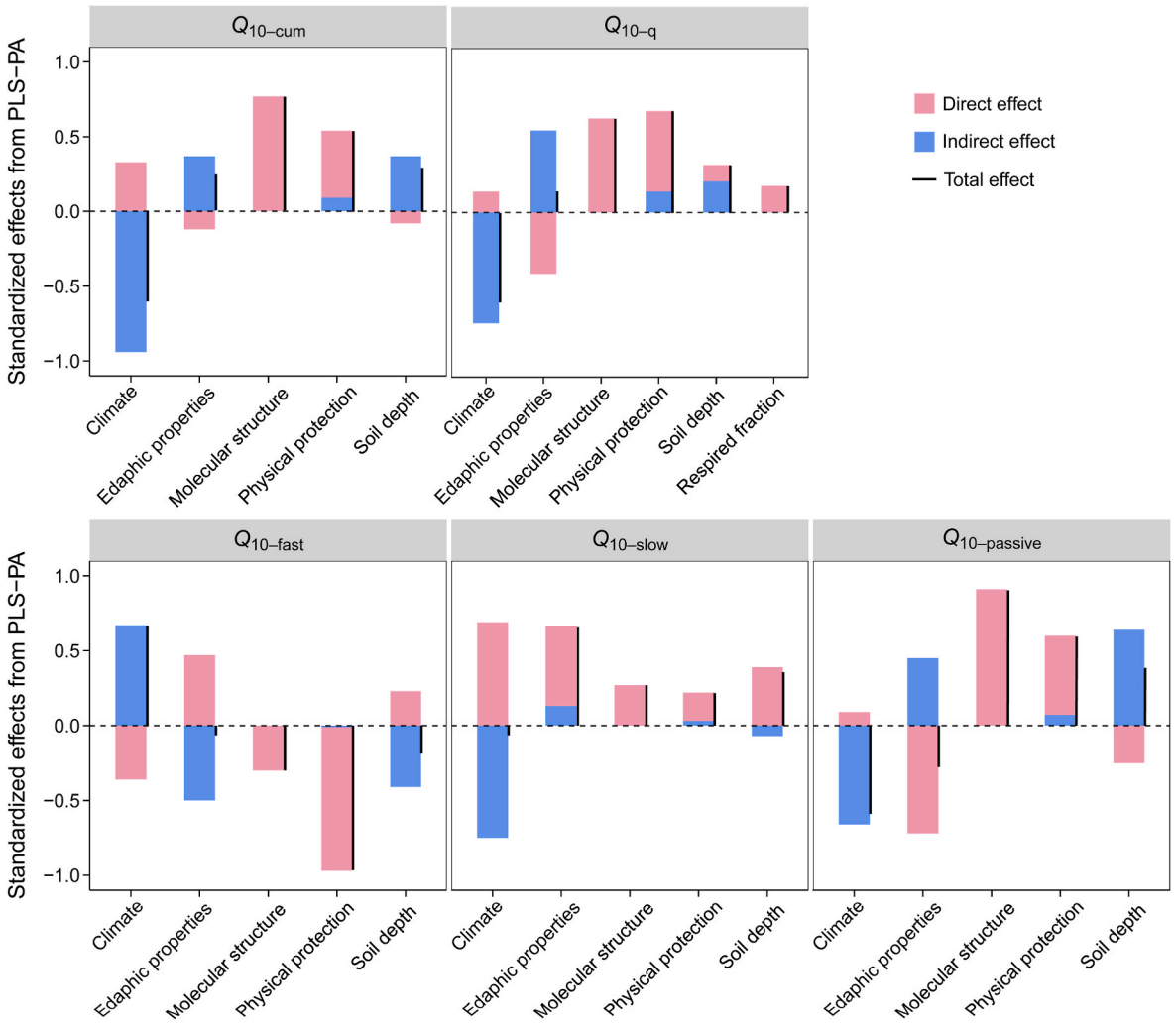

Fig. 8. Standardized direct, indirect, and total effects of latent variables in the path analyses for five Q_{10} metrics. Total effect is defined as the sum of direct and indirect effects.

climate warming, baseline climatic conditions and their controlling of soil physiochemical environmental conditions and chemical structure of SOC compounds must be simultaneously considered in order to provide reliable predictions of profile SOC dynamics.

4.4. Limitations and uncertainties

Although we explicitly assessed potential regulators of Q_{10} relating to chemical composition and physiochemical stability of SOC through soil depths and among vegetation types along a 2500 m elevation transect, we note some limitations and/or uncertainties of our investigation. First, the incubation, like all laboratory incubation experiments, cannot fully captures the real environmental gradient existed along soil profile in situ. For example, decreasing O_2 concentration with increasing soil depth may be common in most soils. Some experiments comparing SOC mineralization under aerobic and anaerobic incubation conditions found that O_2 level is a significant factor regulating temperature sensitivity of microbial mineralization via mediating microbial metabolism and SOC substrate use strategies (Keiluweit et al., 2017; Huang et al., 2020). Second, we did not explicitly investigate the role of microbes such as their metabolism and activity in regulating Q_{10}. Additional consideration of microbial processes (e.g., microbial enzyme activity, community structure and/or carbon use efficiency) would further improve the interpretation of the variability of Q_{10} (Walker et al., 2018; Qin et al., 2021; Xu et al., 2021). At the same study region, indeed, Xu et al. (2021) found that microbial diversity and community composition play an important role in stabilizing SOC decomposition across soil depths. However, here we would like to point out that there would have complex interconnections among chemical composition, physical protection and microbial activities in regulating SOC decomposition and its response to climate change. Third, the incubation was relatively short (i.e., 128 days) and did not enable the three-pool carbon model to reliably infer decay rate for the passive pool with long turnover time and thus its Q_{10} (Jian et al., 2020). As expected, the model predicted larger variability of Q_{10} for the passive pool than for the fast and slow pools (Fig. 1). The stability of passive pool may be with the involvement of various soil physiochemical protection processes, including trade-offs between chemical composition and physical protection.

4.5. Conclusions

By assessing Q_{10} values of SOC decomposition observed by incubating (128 days) soils from five soil layer depths down to 1 m in various vegetation types along a ~2500 m elevational gradient, we provided new evidence that Q_{10} is less varied through soil profile, but has significant difference among vegetation types. In general, SOC decomposition was more sensitive to temperature changes in higher-altitude sites where have lower temperature, confirming the expectation that SOC in colder regions (e.g., permafrost tundra systems and alpine ecosystems) might be more vulnerable to global warming (Koven et al., 2017; Wang

et al., 2019; Lei et al., 2021). Both chemical composition and soil physiochemical protection of SOC were identified to have direct effect on Q_{10} across the elevation gradient. Specifically, Q_{10} was notably positively correlated to the ratio of hydrophobic to hydrophilic organic carbon substrates, and to the ratio of alkyl C to O-alkyl C, demonstrating that chemically recalcitrant SOC pools are more sensitive to temperature. Together with inhibited soil weathering and thus less physiochemical stabilization of SOC against decomposition, this can explain why SOC in cold regions is more sensitive to warming. Indeed, the role of climate manifests when its effects on chemical composition and physiochemical protection are considered. Climate reflected by elevation and depth-specific soil temperature could explain ~80% of the variance of either chemical composition or physiochemical stability across the soil depths and elevation gradient. Overall, our study revealed spatially heterogeneous temperature sensitivity of SOC decomposition, which is largely controlled by climate-induced variability of both chemical recalcitrance and physiochemical protection of SOC. Baseline climatic condition (which largely determines vegetation type and thus the quantity and quality of carbon inputs) and its direct and indirect effects on chemical recalcitrance and physiochemical protection of SOC must be properly considered in Earth system models in order to reliably predict SOC dynamics in response to global warming.

Author contributions

Z.L. designed the study and led field sampling with the contribution of all authors, X.M. performed laboratory measurements and incubation, J.Z. assessed the data, Z.L. led manuscript writing and interpreted the results with the contribution of X.M., J.Z. and all authors.

Declaration of competing interest

The authors declare that they have no known competing financial interests or personal relationships that could have appeared to influence the work reported in this paper.

Data availability statement

The data is available from the corresponding author upon reasonable request.

Acknowledgements

This study is financially supported by the National Natural Science Foundation of China (grant no. 41930754, 32171639), national key research program of Ministry of Science and Technology of China (grant no. 2021YFE0114500), and Fundamental Research Funds for the Central Universities (226-2022-00084).

Appendix A. Supplementary data

Supplementary data to this article can be found online at https://doi.org/10.1016/j.soilbio.2022.108743.

References

Aerts, R., 1997. Climate, leaf litter chemistry and leaf litter decomposition in terrestrial ecosystems: a triangular relationship. Oikos 79, 439–449. https://doi.org/10.2307/3546886.

Borcard, D., Gillet, F., Legendre, P., 2011. Numerical Ecology with R. Springer.

Brooks, S.P., Gelman, A., 1998. General methods for monitoring convergence of iterative simulations. Journal of Computational & Graphical Statistics 7, 434–455. https://doi.org/10.2307/1390675.

Conant, R.T., Drijber, R.A., Haddix, M.L., Parton, W.J., Paul, E.A., Plante, A.F., Six, J., Steinweg, J.M., 2008. Sensitivity of organic matter decomposition to warming varies with its quality. Global Change Biology 14, 868–877. https://doi.org/10.1111/j.1365-2486.2008.01541.x.

Cordova, S.C., Olk, D.C., Dietzel, R.N., Mueller, K.E., Archontouilis, S.V., Castellano, M. J., 2018. Plant litter quality affects the accumulation rate, composition, and stability of mineral-associated soil organic matter. Soil Biology and Biochemistry 125, 115–124. https://doi.org/10.1016/j.soilbio.2018.07.010.

Cotrufo, M.F., Ranalli, M.G., Haddix, M.L., Six, J., Lugato, E., 2019. Soil carbon storage informed by particulate and mineral-associated organic matter. Nature Geoscience 12, 989–994. https://doi.org/10.1038/s41561-019-0484-6.

Coûteaux, M.-M., Bottner, P., Berg, B., 1995. Litter decomposition, climate and liter quality. Trends in Ecology & Evolution 10, 63–66. https://doi.org/10.1016/S0169-5347(00)88978-8.

Davidson, E.A., Janssens, I.A., 2006. Temperature sensitivity of soil carbon decomposition and feedbacks to climate change. Nature 440, 165–173. https://doi.org/10.1038/nature04514.

Djukic, I., Zehetner, F., Mentler, A., Gerzabek, M.H., 2010. Microbial community composition and activity in different Alpine vegetation zones. Soil Biology and Biochemistry 42, 155–161. https://doi.org/10.1016/j.soilbio.2009.10.006.

Doetterl, S., Berhe, A.A., Arnold, C., Bodé, S., Fiener, P., Finke, P., Fuchslueger, L., Griepentrog, M., Harden, J.W., Nadeu, E., Schnecker, J., Six, J., Trumbore, S., Van Oost, K., Vogel, C., Boeckx, P., 2018. Links among warming, carbon and microbial dynamics mediated by soil mineral weathering. Nature Geoscience 11, 589–593. https://doi.org/10.1038/s41561-018-0168-7.

Doetterl, S., Stevens, A., Six, J., Merckx, R., Van Oost, K., Casanova Pinto, M., Casanova-Katny, A., Muñoz, C., Boudin, M., Zagal Venegas, E., Boeckx, P., 2015. Soil carbon storage controlled by interactions between geochemistry and climate. Nature Geoscience 8, 780–783. https://doi.org/10.1038/NGEO2516.

Dungait, J.A., Hopkins, D.W., Gregory, A.S., Whitmore, A.P., 2012. Soil organic matter turnover is governed by accessibility not recalcitrance. Global Change Biology 18, 1781–1796. https://doi.org/10.1111/j.1365-2486.2012.02665.x.

Freschet, G.T., Valverde-Barrantes, O.J., Tucker, C.M., Craine, J.M., McCormack, M.L., Violle, C., Fort, F., Blackwood, C.B., Urban-Mead, K.R., Iversen, C.M., Bonis, A., Comas, L.H., Cornelissen, J.H.C., Dong, M., Guo, D.L., Hobbie, S.E., Holdaway, R.J., Kembel, S.W., Makita, N., Onipchenko, V.G., Picon-Cochard, C., Reich, P.B., de la Riva, E.G., Smith, S.W., Soudzilovskaia, N.A., Tjoelker, M.G., Wardle, D.A., Roumet, C., 2017. Climate, soil and plant functional types as drivers of global fine-root trait variation. Journal of Ecology 105, 1182–1196. https://doi.org/10.1111/1365-2745.12769.

Guan, S., An, N., Zong, N., He, Y.T., Shi, P., Zhang, J.J., He, N.P., 2018. Climate warming impacts on soil organic carbon fractions and aggregate stability in a Tibetan alpine meadow. Soil Biology and Biochemistry 116, 224–236. https://doi.org/10.1016/j.soilbio.2017.10.011.

Haaf, D., Six, J., Doetterl, S., 2021. Global patterns of geo-ecological controls on the response of soil respiration to warming. Nature Climate Change 11, 623–627. https://doi.org/10.1038/s41558-021-01068-9.

Hall, S.J., Ye, C., Weintraub, S.R., Hockaday, W.C., 2020. Molecular trade-offs in soil organic carbon composition at continental scale. Nature Geoscience 13, 687–692. https://doi.org/10.1038/s41561-020-0634-x.

He, N., Wang, R., Gao, Y., Dai, J., Wen, Yu G., 2013. Changes in the temperature sensitivity of SOM decomposition with grassland succession: implications for soil C sequestration. Ecology and Evolution 3, 5045–5054. https://doi.org/10.1002/ece3.881.

Hemingway, J.D., Rothman, D.H., Grant, K.E., Rosengard, S.Z., Eglinton, T.I., Derry, L.A., Galy, V.V., 2019. Mineral protection regulates long-term global preservation of natural organic carbon. Nature 570, 228–231. https://doi.org/10.5281/zenodo.1158742.

Hicks Pries, C.E., Castanha, C., Porras, R.C., Torn, M.S., 2017. The whole-soil carbon flux in response to warming. Science 355, 1420–1423. https://doi.org/10.1126/science.aal1319.

Huang, W., Ye, C., Hockaday, W.C., Hall, S.J., 2020. Trade-offs in soil carbon protection mechanisms under aerobic and anaerobic conditions. Global Change Biology 26, 3726–3737. https://doi.org/10.1111/gcb.15100.

Jackson, R.B., Lajtha, K., Crow, S.E., Hugelius, G., Kramer, M.G., Pineiro, G., 2017. The ecology of soil carbon: pools, vulnerabilities, and biotic and abiotic controls. Annual Review of Ecology Evolution and Systematics 48, 419–445. https://doi.org/10.1146/annurev-ecolsys-112414-054234.

Jian, S., Li, J., Wang, G., Kluber, L.A., Mayes, M.A., 2020. Multi-year incubation experiments boost confidence in model projections of long-term soil carbon dynamics. Nature Communications 11, 5864. https://doi.org/10.1038/s41467-020-19428-y.

Jobbagy, E.G., Jackson, R.B., 2000. The vertical distribution of soil organic carbon and its relation to climate and vegetation. Ecological Applications 10, 423–436. https://doi.org/10.1890/1051-0761(2000)010[0423:TVDOSO]2.0.CO;2.

Keiluweit, M., Wanzek, T., Kleber, M., Nico, P., Fendorf, S., 2017. Anaerobic microsites have an unaccounted role in soil carbon stabilization. Nature Communications 8, 1771. https://doi.org/10.1038/s41467-017-01406-6.

Koven, C.D., Hugelius, G., Lawrence, D.M., Wieder, W.R., 2017. Higher climatological temperature sensitivity of soil carbon in cold than warm climates. Nature Climate Change 7, 817–822. https://doi.org/10.1038/NCLIMATE3421.

Kreyling, J., Schweiger, A.H., Bahn, M., Ineson, P., Migliavacca, M., Morel-Journel, T., Christiansen, J.R., Schtickzelle, N., Larsen, K.S., 2018. To replicate, or not to replicate–that is the question: how to tackle nonlinear responses in ecological experiments. Ecology Letters 21, 1629–1638. https://doi.org/10.1111/ele.13134.

Lavallee, J.M., Soong, J.L., Cotrufo, M.F., 2020. Conceptualizing soil organic matter into particulate and mineral-associated forms to address global change in the 21st century. Global Change Biology 26, 261–273. https://doi.org/10.1111/gcb.14859.

Lei, J., Guo, X., Zeng, Y., Zhou, J., Gao, Q., Yang, Y., 2021. Temporal changes in global soil respiration since 1987. Nature Communications 12, 403. https://doi.org/10.1038/s41467-020-20616-z.

Li, J., Pei, J., Pendall, E., Reich, P.B., Noh, N.J., Li, B., Fang, C., Nie, M., 2020. Rising temperature may trigger deep soil carbon loss across forest ecosystems. Advanced Science 7, 2001242. https://doi.org/10.1002/advs.202001242.

Li, J., Yan, D., Pendall, E., Pei, J., Noh, N.J., He, J.-S., Li, B., Nie, M., Fang, C., 2018. Depth dependence of soil carbon temperature sensitivity across Tibetan permafrost regions. Soil Biology and Biochemistry 126, 82–90. https://doi.org/10.1016/j.soilbio.2018.08.015.

Li, J., Zhang, Q., Li, Y., Liu, Y., Xu, J., Di, H., 2017. Effects of long-term mowing on the fractions and chemical composition of soil organic matter in a semiarid grassland. Biogeosciences 14, 2685. https://doi.org/10.5194/bg-14-2685-2017.

Li, X.L., Gai, J.P., Cai, X.B., Li, X.L., Christie, P., Zhang, F.S., Zhang, J.L., 2014. Molecular diversity of arbuscular mycorrhizal fungi associated with two co-occurring perennial plant species on a Tibetan altitudinal gradient. Mycorrhiza 24, 95–107. https://doi.org/10.1007/s00572-013-0518-7.

Liang, C., Amelung, W., Lehmann, J., Kästner, M., 2019. Quantitative assessment of microbial necromass contribution to soil organic matter. Global Change Biology 25, 3578–3590. https://doi.org/10.1111/gcb.14781.

Liu, Y., He, N.P., Zhu, J.X., Xu, L., Yu, G.R., Niu, S.L., Sun, X.M., Wen, X.F., 2017. Regional variation in the temperature sensitivity of soil organic matter decomposition in China's forests and grasslands. Global Change Biology 23, 3393–3402. https://doi.org/10.1111/gcb.13613.

Lugato, E., Lavallee, J.M., Haddix, M.L., Panagos, P., Cotrufo, M.F., 2021. Different climate sensitivity of particulate and mineral-associated soil organic matter. Nature Geoscience 14, 295–300. https://doi.org/10.1038/s41561-021-00744-x.

Luo, Z., Viscarra Rossel, R.A., Shi, Z., 2020. Distinct controls over the temporal dynamics of soil carbon fractions after land use change. Global Change Biology 26, 4614–4625. https://doi.org/10.1111/gcb.15157.

Mueller, C.W., Rethemeyer, J., Kao-Kniffin, J., Löppmann, S., Hinkel, K.M., Bockheim, J. G., 2015. Large amounts of labile organic carbon in permafrost soils of northern A laska. Global Change Biology 21, 2804–2817. https://doi.org/10.1111/gcb.12876.

Nottingham, A.T., Whitaker, J., Ostle, N.J., Bardgett, R.D., McNamara, N.P., Fierer, N., Salinas, N., Ccahuana, A.J., Turner, B.L., Meir, P., 2019. Microbial responses to warming enhance soil carbon loss following translocation across a tropical forest elevation gradient. Ecology Letters 22, 1889–1899. https://doi.org/10.1111/ele.13379.

Pei, J.M., Yan, D., Li, J.Q., Qiong, L., Yang, Y.W., Fang, C.M., Wu, J.H., 2022. Alpine meadow degradation enhances the temperature sensitivity of soil carbon decomposition on the Qinghai-Tibetan plateau. Applied Soil Ecology 170, 104290. https://doi.org/10.1016/j.apsoil.20- 21.104290.

Poeplau, C., Kätterer, T., Leblans, N.I., Sigurdsson, B.D., 2017. Sensitivity of soil carbon fractions and their specific stabilization mechanisms to extreme soil warming in a subarctic grassland. Global Change Biology 23, 1316–1327. https://doi.org/10.1111/gcb.13491.

Qin, S., Chen, L., Fang, K., Zhang, Q., Wang, J., Liu, F., Yu, J., Yang, Y., 2019. Temperature sensitivity of SOM decomposition governed by aggregate protection and microbial communities. Science Advances 5, eaau1218. https://doi.org/10.1126/sciadv.aau1218.

Qin, S., Kou, D., Mao, C., Chen, Y., Chen, L., Yang, Y., 2021. Temperature sensitivity of permafrost carbon release mediated by mineral and microbial properties. Science Advances 7, eabe3596. https://doi.org/10.1126/sciadv.abe3596.

R Development Core Team, 2021. R: A Language and Environment for Statistical Computing. R Foundation for Statistical Computing, Vienna, Austria.

Schmidt, M.W., Torn, M.S., Abiven, S., Dittmar, T., Guggenberger, G., Janssens, I.A., Kleber, M., Kögel-Knabner, I., Lehmann, J., Manning, D.A., 2011. Persistence of soil organic matter as an ecosystem property. Nature 478, 49–56. https://doi.org/10.1038/nature10386.

Six, J., Elliott, E.T., Paustian, K., Doran, J.W., 1998. Aggregation and soil organic matter accumulation in cultivated and native grassland soils. Soil Science Society of America Journal 62, 1367–1377. https://doi.org/10.2136/sssaj1998.03615995006200050032x.

Vance, E.D., Brookes, P.C., Jenkinson, D.S., 1987. An extraction method for measuring soil microbial biomass C. Soil Biology and Biochemistry 19, 703–707. https://doi.org/10.1016/0038-0717(87)90052-6.

Vaughn, L.J., Torn, M.S., 2019. 14 C evidence that millennial and fast-cycling soil carbon are equally sensitive to warming. Nature Climate Change 9, 467–471. https://doi.org/10.1038/s41558-019-0468-y.

Vrugt, J.A., Ter Braak, C.J.F., 2011. DREAM((D)): an adaptive Markov chain Monte Carlo simulation algorithm to solve discrete, noncontinuous, and combinatorial posterior parameter estimation problems. Hydrology and Earth System Sciences 15, 3701–3713. https://doi.org/10.5194/hess-15-3701-2011.

Wagai, R., Kishimoto-Mo, A.W., Yonemura, S., Shirato, Y., Hiradate, S., Yagasaki, Y., 2013. Linking temperature sensitivity of soil organic matter decomposition to its molecular structure, accessibility, and microbial physiology. Global Change Biology 19, 1114–1125. https://doi.org/10.1111/gcb.12112.

Walker, T.W.N., Kaiser, C., Strasser, F., Herbold, C.W., Leblans, N.I.W., Woebken, D., Janssens, I.A., Sigurdsson, B.D., Richter, A., 2018. Microbial temperature sensitivity and biomass change explain soil carbon loss with warming. Nature Climate Change 8, 885–889. https://doi.org/10.1038/s41558-018-0259-x.

Wang, C., Qu, L., Yang, L., Liu, D., Morrissey, E., Miao, R., Liu, Z., Wang, Q., Fang, Y., Bai, E., 2021. Large-scale importance of microbial carbon use efficiency and necromass to soil organic carbon. Global Change Biology 27, 2039–2048. https://doi.org/10.1111/gcb.15550.

Wang, D., Wu, T.H., Zhao, L., Mu, C.C., Li, R., Wei, X.H., Hu, G.J., Zou, D.F., Zhu, X.F., Chen, J., Hao, J.M., Ni, J., Li, X.F., Ma, W.S., Wen, A.M., Shang, C.P., La, Y.N., Ma, X., Wu, X.D., 2021. A 1 km resolution soil organic carbon dataset for frozen ground in the Third Pole. Earth System Science Data 13, 3453–3465. https://doi.org/10.5194/essd-13-3453-2021.

Wang, J.S., Sun, J., Yu, Z., Li, Y., Tian, D.S., Wang, B.X., Li, Z.L., Niu, S.L., 2019. Vegetation type controls root turnover in global grasslands. Global Ecology and Biogeography 28, 442–455. https://doi.org/10.1111/geb.12866.

Wang, Q., Zhao, X., Chen, L., Yang, Q., Chen, S., Zhang, W., 2019. Global synthesis of temperature sensitivity of soil organic carbon decomposition: latitudinal patterns and mechanisms. Functional Ecology 33, 514–523. https://doi.org/10.1111/1365-2435.13256.

Xu, M., Li, X., Kuyper, T.W., Xu, M., Li, X., Zhang, J., 2021. High microbial diversity stabilizes the responses of soil organic carbon decomposition to warming in the subsoil on the Tibetan Plateau. Global Change Biology 27, 2061–2075. https://doi.org/10.1111/gcb.15553.